INITIAL POSTBUCKLING BEHAVIOR OF STIFFENED CYLINDRICAL SHELLS

by

D. O. Brush, Consultant

LMSC 6-77-67-52 November 1967

Aerospace Sciences Laboratory
Lockheed Missiles and Space Company
Palo Alto, California

FOREWORD

D. O. Brush is Professor of Engineering and Chairman of the Department of Civil Engineering at the University of California at Davis. The major portion of this work was carried out as part of his consulting activities with the Solid Mechanics group of the Aerospace Sciences Laboratory. The work was funded under the Lockheed Independent Research Program.

ABSTRACT

A theory developed by W. T. Koiter for the initial postbuckling behavior of thin-walled shells is applied in an analysis of the imperfection sensitivity of ring-and-stringer stiffened cylinders subjected to axial compression. The cylinders are considered to be simply supported, and both eccentricity and torsional rigidity of stiffeners are taken into account. Values of a so-called imperfection sensitivity parameter are determined for particular stiffened cylinders, and the suitability of the parameter as a practical measure of imperfection sensitivity is examined. Theoretical results are correlated with available data for the experimental buckling loads of stringer stiffened cylinders. The evidence for the suitability of the parameter as a practical measure of imperfection sensitivity is judged to be promising but not conclusive.

ACKNOWLEDGMENTS

The author is indebted to F. A. Brogan for conversion of the equations to finite difference form and for the computer program, and to B. O. Almroth and K. J. Forsberg for their support of the investigation.

CONTENTS

LIST OF FIGURES

LIST OF TABLES

NOTATION

A_s, A_r	cross-sectional area of stringers and rings, respectively
A, B, D	Eq. (2)
C	buckle mode amplitude as a fraction of cylinder radius
C^*	imperfection amplitude as a fraction of cylinder radius
E, E_s, E_r	Young's modulus, skin, stringer, and ring, respectively
I_s, I_r	stiffener moments of inertia relative to skin middle surface
J_s, J_r	torsional moments of inertia
L	cylinder length
N_{x0}, N_{y0}, N_{xy0}	prebuckling membrane forces (lb/in)
R	middle surface radius
S	imperfection sensitivity parameter, Eq. (6)
$\bar{V}$	nondimensional total potential energy
U_0, W_0, U_1, V_1, W_1	displacement parameters, Eq. (A25)
e_s, e_r	distance from shell middle surface to stiffener centroid - positive for external stiffener
$\bar{m}$, n	axial and circumferential buckle wave length parameters
m	$= \bar{m}\pi R/L$
r	ring spacing
s	stringer spacing
t	skin thickness
u, v, w	nondimensional displacement components of a point on shell middle surface - normalized with respect to R; w positive outward

w^*	initial deviation from cylindrical form
x, y	nondimensional axial and circumferential coordinates
z	nondimensional radial coordinate measured from middle surface - positive outward
$\alpha_1, \ldots, \alpha_7$	orthotropy parameters (Eq. 3)
γ^2	$= (t/R)^2/12$
$\epsilon_x, \epsilon_y, \gamma_{xy}$	middle surface strain components
$\kappa_x, \kappa_y, \kappa_{xy}$	middle surface curvature changes and twist
$\lambda_x, \lambda_y, \lambda_{xy}$	nondimensional applied-load parameters (Eq. A13)
λ_{CL}	classical critical value of λ_x
λ_M	maximum value of λ_x on load-displacement curve for initially imperfect cylinder
ν, ν_s, ν_r	Poisson's ratio, skin, stringer, and ring, respectively
ω_x, ω_y	rotations about x and y coordinate lines, respectively

1. INTRODUCTION

Buckling load calculations based on classical stability theory for axially compressed cylindrical shells seem to be in reasonably close agreement with test data for heavily stiffened cylinders. For lightly stiffened or monocoque cylinders, on the other hand, theoretical and experimental values may differ by as much as a factor of five. The principal cause of the uncertain correlation is now agreed to be small imperfections in the initial shape of the shell. Since initial imperfections are inevitable in all shells, monocoque cylinders apparantly are more sensitive to such imperfections than are heavily stiffened cylinder. Consequently, degree of imperfection sensitivity is an important factor in shell design.

An analysis of imperfection sensitivity for shells of arbitrary shape is included in a general theory of initial postbuckling behavior presented by Koiter in Refs. 1 and 2. Koiter applied the theory to the monocoque cylindrical shell in those references, and to a simply supported cylindrical panel in Ref. 3. More recently the theory has been applied in the analysis of a variety of shell configurations and loadings by Budiansky, Hutchinson, and Amazigo in the Division of Engineering and Applied Physics at Harvard (e.g., Refs. 4 and 5). Reference 5, in particular, reports an excellent and extensive investigation of the ring-and-stringer stiffened cylinder subjected to axial and hydrostatic pressure loadings.

The present report represents an independent application of the Koiter theory to the axially compressed, stiffened cylinder. It differs from that in Ref. 5 in several respects. (1) The analysis is based on a somewhat different formulation of the basic shell equations that takes into account influence of stiffener torsional rigidity. Inclusion is found to affect the imperfection sensitivity parameter by as much as a factor of two in practical cases. (2) Finite differences instead of the Galerkin procedure are utilized in the numerical analysis. Where the two investigations overlap, numerical results are the same. (3) Numerical results are presented only for the case of stringer-stiffened cylinders, but the practical significance of the results for that case is examined in greater detail.

2. THE KOITER THEORY

The principal result of the Koiter postbuckling behavior theory is illustrated in the load-displacement curves of Figs. 1 and 2. Figure 1 depicts applied-load vs. lateral-displacement relationships for a wide class of initially perfect structures. Parts (a), (b), and (c), respectively, are typical of the behavior under axial loading of flat plates, columns, and certain cylindrical panels. Since each point on the curves represents an equilibrium configuration, the curves themselves are called equilibrium paths. Bifurcation or branch points on the equilibrium paths are denoted by small circles.

Classical stability theory is devoted to the determination of the bifurcation points. Thus it reveals the point at which a second branch starts, but it gives no information about the shape of the second branch. The principal objective of the Koiter theory is the determination of the curvature of the second branch at the bifurcation point.

The relationship of these load-displacement curves to imperfection sensitivity is illustrated in Fig. 2. The curves for initially perfect structures again are shown, together with curves for the corresponding, initially imperfect structures. (These curves may be seen to illustrate the familiar fact that certain kinds of structures buckle gradually, and others abruptly or explosively.) The most important feature of these plots is the appearance of a maximum point on the curve for the imperfect

structure in Fig. 2(c). This maximum point represents a critical load for the structure, and it may be significantly lower than the bifurcation point load of the corresponding perfect structure. Thus we see that structures whose load-displacement curves are of the form of those in Fig. 1(c) are sensitive to the presence of initial imperfections, whereas those of the form of Figs. 1(a) and (b) are not.

The Koiter theory also furnishes an approximate equation for the equilibrium path of the imperfect structure in Fig. 2(c). The equation is based on the simplifying assumption that the initial imperfection is of the form of the classical critical buckle mode for the structure. The equation shows that magnitude of critical load, as represented by the maximum point on the equilibrium path, is a function of: (1) the amplitude of the initial imperfection, and (2) the sharpness of curvature of the equilibrium path of the corresponding perfect structure. The equation is only approximate. However, Koiter presents strong evidence in Ref. 6 that, for the monocoque cylinder at least, the values are rather accurate for lateral displacements as large as the shell wall thickness. A typical plot of critical load vs. imperfection amplitude for a given value of path curvature is shown in Fig. 3(a). The curve is seen to have a vertical tangent at the left end, indicating that even a small imperfection can substantially reduce the magnitude of the critical load. Similarly, a typical plot of critical load vs. path curvature for a given value of imperfection amplitude is shown in Fig. 3(b). The curve clearly illustrates that sharpness of curvature of the secondary equilibrium path is a measure of degree of sensitivity to a given imperfection.

In summary, the Koiter theory furnishes an accurate value for the curvature of the secondary equilibrium path at the bifurcation point. The sign of that value determines whether or not the structure is sensitive to initial imperfections. Second, the Koiter theory furnishes an approximate analysis which shows that, at least for the class of imperfections examined, the sharpness of curvature is a measure of the degree of imperfection sensitivity.

3. APPLICATION TO THE STIFFENED CYLINDRICAL SHELL

Details of the application to the stiffened cylindrical shell are given in the Appendix. The ring-and-stringer stiffened cylinder with simple-support ends is treated. The analysis is based on the Baruch-Singer formulation (Ref. 7) of the basic shell equations. In that formulation, orthotropic shell theory is used to represent the stiffened shell, and stiffener eccentricity is taken into account.

3.1 Classical Stability Equations

The classical stability analysis gives the following expression for the critical value of the applied load parameter λ_x for asymmetric buckling:

$$\lambda_{CL} = \left[-\left(\alpha_5 m^4 + \alpha_7 m^2 n^2 + \alpha_6 n^4 + \alpha_4 + 2\alpha_2 n^2\right) + \left(\alpha_1 m^3 + \nu m\right) A + \left(\alpha_2 n^3 + \alpha_4 n\right) B \right] \div m^2 \tag{1}$$

where

$$A = \left[\frac{1-\nu}{2} \alpha_1 m^5 + \alpha_1 \alpha_4 m^3 n^2 + \nu \frac{1-\nu}{2} m^3 - \frac{1-\nu}{2} mn^2 - \frac{1+\nu}{2} \alpha_2 mn^4 \right] \div D$$

$$B = \left[-\frac{1+\nu}{2} \alpha_1 m^4 n + \left(\alpha_3 \alpha_4 - \frac{1+\nu}{2} \nu\right) m^2 n + \alpha_2 \alpha_3 m^2 n^3 + \frac{1-\nu}{2} \alpha_4 n^3 + \frac{1-\nu}{2} \alpha_2 n^5 \right] \div D \tag{2}$$

$$D = \frac{1-\nu}{2} \alpha_3 m^4 + \left(\alpha_3 \alpha_4 - \nu\right) m^2 n^2 + \frac{1-\nu}{2} \alpha_4 n^4$$

The parameter $m = \bar{m}\pi R/L$, and $\bar{m}$ and n are integers greater than 0 and 1, respectively. The $\bar{m}$ and n are determined by trial in the usual manner to yield the minimum λ_{CL}. For axisymmetric buckling,

$$\lambda_{CL} = \left[- \alpha_5 m^4 - \alpha_4 + \left(\alpha_1 m^2 + \nu \right)^2 / \alpha_3 \right] \div m^2 \tag{3}$$

The α_i are orthotropy parameters given by the following relations:

<u>eccentricity parameters</u>

$$\alpha_1 = \left(1 - \nu^2\right) \frac{A_s}{st} \frac{e_s}{R} \frac{E_s}{E} \quad , \quad \alpha_2 = \left(1 - \nu^2\right) \frac{A_r}{rt} \frac{e_r}{R} \frac{E_r}{E}$$

<u>extensional stiffness parameters</u>

$$\alpha_3 = 1 + \left(1 - \nu^2\right) \frac{A_s}{st} \frac{E_s}{E} \quad , \quad \alpha_4 = 1 + \left(1 - \nu^2\right) \frac{A_r}{rt} \frac{E_r}{E} \tag{4}$$

<u>bending stiffness parameters</u>

$$\alpha_5 = \gamma^2 + \left(1 - \nu^2\right) \frac{I_s}{stR^2} \frac{E_s}{E} \, , \quad \alpha_6 = \gamma^2 + \left(1 - \nu^2\right) \frac{I_r}{rtR^2} \frac{E_r}{E}$$

<u>torsional stiffness parameter</u>

$$\alpha_7 = 2\gamma^2 + \frac{1 - \nu^2}{2tR^2} \left(\frac{1}{1 + \nu_s} \frac{J_s}{s} \frac{E_s}{E} + \frac{1}{1 + \nu_r} \frac{J_r}{r} \frac{E_r}{E} \right)$$

where $\gamma^2 = (t/r)^2/12$. The notation here follows that in an unpublished work by Dr. E. V. Pittner of Lockheed Missiles and Space Company. These stability equations are the same as corresponding equations by Baruch and Singer in Ref. 7.

3.2 Postbuckling Equilibrium - Initially Perfect Cylinders

The postbuckling analysis in the Appendix gives the following equation for the secondary equilibrium path of the initially perfect cylinder, for sufficiently small lateral displacements:

$$\lambda_x/\lambda_{CL} = 1 - SC^2 \tag{5}$$

where C is amplitude of buckle displacement as a fraction of cylinder radius. The coefficient S is here called the imperfection-sensitivity parameter. Its sign determines whether the secondary equilibrium path curves upward or downward from the bifurcation point. Positive values of S are seen to denote imperfection-sensitive structures. A plot based on Eq. (5) of λ_x/λ_{CL} versus C for selected values of S is shown in Fig. 4. For convenience, values are shown only for $C > 0$.

The magnitude of the parameter S is given by the equation (Eq. A28)

$$S = \frac{1}{m^2 \lambda_{CL}} \left[\frac{1}{32} \left(9a_4 m^4 + 2m^2 n^2 + 9a_4 n^4 \right) + \frac{2R}{\pi L} P \right] \tag{6}$$

where P represents the stationary value of a certain functional,

$$\Psi_2 = \int_0^{L/R} F\left(U_0', W_0, U_1, V_1, W_1 \right) dx \tag{7}$$

The magnitude of P is determined as follows. From Eq. (A25),

$$\Psi_2 = \left(P_2^0\left[u_2\right] + \lambda_{CL} P_2^1\left[u_2\right]\right) + P_{21}\left[u_1, u_2\right] C^2 \tag{8}$$

where

$$\begin{aligned} P_2^0\left[u_2\right] = \pi \int_0^{L/R} \Big[& 2\alpha_3 U_0'^2 + 4\nu U_0' W_0 \\ & - 4\alpha_1 U_0' W_0'' + 2(1-\nu)n^2 U_1^2 \\ & - 2(1-\nu)n U_1 V_1' + \alpha_3 U_1'^2 + 4\nu n U_1' V_1 \\ & + 2\nu U_1' W_1 - 2\alpha_1 U_1' W_1'' \\ & + 4\alpha_4 n^2 V_1^2 + (4n\alpha_4 + 16n^3\alpha_2) V_1 W_1 \\ & + \frac{1-\nu}{2} V_1'^2 + 2\alpha_4 W_0^2 + 2\alpha_5 W_0''^2 \\ & + (\alpha_4 + 8\alpha_2 n^2 + 16\alpha_6 n^4) W_1^2 \\ & - 8\nu\gamma^2 n^2 W_1 W_1'' + 4(\alpha_7 - 2\nu\gamma^2) n^2 W_1'^2 \\ & + \alpha_5 W_1''^2 \Big] dx \end{aligned} \tag{9}$$

$$P_2^1\left[u_2\right] = \pi \int_0^{L/R} \left[2 W_0'^2 + W_1'^2\right] dx$$

$$P_{21}\left[u_1 , u_2\right]$$

$$= \frac{\pi}{4}\int_0^{L/R} \Big\{ \Big[2(\alpha_3 m^2 + \nu n^2) + 2(\alpha_3 m^2 - \nu n^2)\cos 2mx\Big] U_0'$$

$$- \Big[2(1 - \nu)mn^2 \sin 2mx\Big] U_1$$

$$- \Big[(\alpha_3 m^2 - \nu n^2) + (\alpha_3 m^2 + \nu n^2)\cos 2mx\Big] U_1'$$

$$+ \Big[2n(\alpha_4 n^2 - \nu m^2) - 2n(\alpha_4 n^2 + \nu m^2)\cos 2mx\Big] V_1$$

$$+ \Big[(1 - \nu)mn \sin 2mx\Big] V_1'$$

$$+ \Big[2(\alpha_4 n^2 + \nu m^2) - 2(\alpha_4 n^2 - \nu m^2)\cos 2mx\Big] W_0$$

$$+ \Big[\big\{4(-\alpha_3 m^2 A + \alpha_1 m^3 - \nu mnB + \nu m)$$

$$+ 2(1 - \nu)(n^2 A + mnB)\big\} \sin 2mx\Big] W_0'$$

$$- \Big[2\alpha_1 m^2 (1 + \cos 2mx)\Big] W_0''$$

$$+ \Big[\big\{(\alpha_4 n^2 - \nu m^2) + 4n^2(\alpha_4 nB - \alpha_4 + \nu mA)$$

$$- 2n(1 - \nu)(mnA + m^2 B)\big\}$$

$$- \big\{(\alpha_4 n^2 + \nu m^2) + 4n^2 (\alpha_4 nB - \alpha_4 + \nu mA)$$

$$+ 2n(1 - \nu)(mnA + m^2 B)\big\} \cos 2mx\Big] W_1$$

$$+ \Big[\big\{2(\alpha_3 m^2 A - \alpha_1 m^3 + \nu mnB - \nu m)$$

$$+ (1 - \nu)(n^2 A + mnB)\big\} \sin 2mx\Big] W_1'$$

$$+ \Big[\alpha_1 m^2 (1 + \cos 2mx)\Big] W_1''\Big\}\, dx \qquad \text{(9 cont'd)}$$

and primes denote differentiation with respect to x.

Values of U_0' , W_0 , U_1 , V_1 , W_1 for stationary ψ_2 may be determined by use of finite differences and numerical integration. If such values are introduced into Eqs. (8) and (9) and the result termed $(\psi_2)_{\text{stationary}}$, P is then given by the equation

$$(\psi_2)_{\text{stationary}} = \frac{1}{2} C^4 P \tag{10}$$

A quantitative comparison based on Eq. (6) of the imperfection sensitivity of lightly and heavily stiffened cylinders is illustrated in Fig. 5. The graph shows the imperfection-sensitivity parameter S plotted against an axial bending stiffness parameter for stringer stiffened cylinders. The examples shown are for symmetrical (i.e., non-eccentric) stringers of rectangular cross-section, with a stringer spacing s = 0.1 R, stringer width equal to 0.01 R, and varying stringer thicknesses. The values of the axial bending stiffness parameter cover the practical design range, from the monocoque shell on the left to a stiffened shell on the right whose axial bending stiffness α_5 is 1000 times that of the corresponding monocoque shell. As expected, the curve indicates that the heavily stiffened cylinder is substantially less sensitive to imperfections than the lightly stiffened one. The curve also shows that the sensitivity parameter diminishes sharply to a rather small value for relatively little stiffening.

A comparison of present numerical results for the sensitivity parameter S with results from Ref. 5 is shown in Fig. 6. The parameter B in Ref. 5 is the same as $-(t/R)^2 S$ in the present notation. The results are seen to be the same in the cases illustrated. Similar agreement was found in other cases investigated.

The Baruch-Singer shell equations on which the present analysis is based take into account stiffener torsional rigidity. A quantitative evaluation of the influence of torsional rigidity on the magnitude of the classical buckling load was presented by Singer, Baruch, and Harari in Table 3 of Ref. 8. The evaluation is based on four examples corresponding to Cylinder Nos. 1 through 4 from the test program reported by Card and Jones in Ref. 9. Neglect of torsional rigidity was found to change the classical buckling load by as much as 20 percent. These same four examples are used in the present report to illustrate the influence of torsional rigidity on the magnitude of the sensitivity parameter S. Results are shown in Table 1. Neglect of torsional rigidity is seen to change the magnitude of S in these examples by as much as 113 percent.

3.3 Initially Imperfect Cylinders

Equation (5) represents the secondary equilibrium path for the initially perfect cylinder. An approximate equation for the equilibrium path of the initially imperfect cylinder is derived in the Appendix for an initial imperfection of the form (Eq. A38)

$$w^* = C^* \sin mx \sin ny \tag{11}$$

where m and n are the classical buckling mode wave length parameters, and C^* represents imperfection amplitude as a fraction of cylinder radius. The equation is found to be

$$\frac{\lambda_x}{\lambda_{CL}} = \frac{1 - SC^2}{1 + C^*/C} \tag{12}$$

For $C^* = 0$, Eq. (12) is the same as Eq. (5). A set of curves based on Eq. (12) for selected values of C^* is shown in Fig. 7. The magnitude of the critical load as represented by the maximum point on each load-displacement curve is seen to decrease markedly as the imperfection amplitude gets larger.

An equation for the maximum load λ_M itself as a function of C^* and S is given in Eq. (A42):

$$\left(1 - \frac{\lambda_M}{\lambda_{CL}}\right)^{3/2} = \frac{3\sqrt{3}}{2} \frac{\lambda_M}{\lambda_{CL}} \sqrt{S} \, |C^*| \quad , \quad S > 0 \tag{13}$$

A plot of λ_M/λ_{CL} versus C^* for selected values of S is shown in Fig. 8, and a plot of λ_M/λ_{CL} versus S for selected values of C^* in Fig. 9. The curves show the expected dependence of the critical load on both imperfection amplitude and imperfection sensitivity.

4. Practical Significance of Results

The value given by the Koiter theory for the parameter S is accurate for sufficiently small displacements from the unbuckled form. However, the argument relating that parameter to the practical matter of imperfection sensitivity has been based on many assumptions. Furthermore, the value of S corresponding to the critical classical buckle mode may be less significant than the value for a slightly different mode. The critical classical buckling load is merely the lowest among a set of eigenvalues. The value of S for a somewhat higher eigenvalue may be much greater than that for the classical load itself. In some cases the buckle mode associated

with a higher than critical eigenvalue for the perfect shell may be the critical mode for the imperfect shell. An example is given in Fig. 10. The curves represent load-displacement relations for a very lightly stiffened cylinder. For the classical mode, $\bar{m} = 3$, $n = 16$, $\lambda_{CL} = -0.001399$, and $S = 96{,}000$. The curves for this mode for both perfect and initially imperfect cylinders (for $C^* = 0.1\ t/R$) are represented by solid lines in Fig. 10. For the mode $\bar{m} = 4$, $n = 17$, the corresponding values are 0.001404 and 176,000. The curves for the second mode are represented by the dotted lines in Fig. 10. It may be seen that, whereas the classical mode gives the lower of the two critical loads for the perfect cylinder, the opposite is true for the imperfect one. This reversal is not apt to occur unless the eigenvalues are close in magnitude, but there is a systematic element of uncertainty.

Whether the parameter S is in fact a satisfactory practical measure of imperfection sensitivity is subject to experimental examination. The plot in Fig. 9 of λ_M/λ_{CL} versus S shows that the curve for a given imperfection amplitude C^* sweeps downward and to the right from the point $\lambda_M/\lambda_{CL} = 1$, $S = 0$. A similar plot of the "best fit" curve from a large amount of suitable test data should have the same form. A plot of test points themselves should scatter about such a downward sweeping curve rather than about a horizontal line, $\lambda_M/\lambda_{CL} = \text{constant}$.

Test data from the literature are given in Table 2 for the buckling of stringer stiffened cylinders. Results are taken from four experimental studies: Card and Jones (Ref. 9); Milligan, Gerard, Lakshmikantham, and Becker (Ref. 10); Peterson and Dow (Ref. 11); and Katz (Ref. 12). The

values of the orthotropy parameters α_1 , ... , α_7 in the table were supplied by E. V. Pittner and B. O. Almroth. Included in the table are calculated values of λ_{CL} and S based on Eqs. (1) and (6), respectively. The last column in the table lists experimental buckling loads normalized with respect to corresponding classical critical values for simply supported cylinders. Values of $\lambda_{exp}/\lambda_{CL}$ versus S from Table 2 are plotted in Fig. 11(a). As may be seen, the test points in Fig. 11(a) do not follow a well defined trend.

One of the obvious difficulties with this representation of the data is that the test cylinders were not simply supported. In Fig. 11(b) the test data are re-plotted in terms of a load parameter $\lambda_{exp}/\lambda_{CL}$ in which the denominator is based on the analysis of clamped-end cylinders in Ref. 13. That analysis also takes into account the influence of nonlinear deformation prior to buckling. The critical-load values based on Ref. 13 were furnished by B. O. Almroth. Of course, the abscissas in Fig. 11(b) necessarily remain the values calculated from Eq. (6) for simple support ends.

Results shown in Fig. 11(b) are promising but not conclusive. Most of the data follow the appropriate downward-sweeping trend, but the Katz data are far out of line. Furthermore, the data from the several investigators do not overlap one another in the parameter S ; additional data are needed. The significance of the comparison would be enhanced by use of test data for simple-support ends or initial postbuckling theory for clamped ends.

It is concluded that additional research is needed before the parameter S can be considered a satisfactory practical measure of imperfection sensitivity for axially compressed, stringer stiffened cylinders.

APPENDIX

Classical stability theory is based on the assumption that, for a loaded structure, two adjacent equilibrium configurations exist for a given value of the applied load, one unbuckled and the other buckled. Consequently, the displacements representing the buckled configuration may be written in the form

$$u = u_0 + u_1 \tag{A1}$$

where u_0 represents the configuration at impending buckling and u_1 is an infinitesimal increment. The u_0 displacements are determined from an auxiliary analysis of the unbuckled form, and the inherently nonlinear equations governing stability are linearized in the incremental displacements u_1.

In an analogous manner, the Koiter theory for initial postbuckling behavior starts from the assumption that, for loads in the neighborhood of the buckling load, a neighboring state of equilibrium exists that may be represented by the displacement

$$u = u_0 + Cu_1 + u_2 \tag{A2}$$

where u_0 is the configuration at impending buckling, u_1 is the buckling mode, C is amplitude of the buckling mode, and u_2 is a small incremental displacement that is in some sense orthogonal to the buckling mode. The displacements u_0 are determined from an auxiliary analysis of the unbuckled

form, the displacements u_1 from an auxiliary classical stability analysis, and the inherently nonlinear equations governing initial postbuckling behavior are linearized in the incremental quantities u_2. Koiter shows in Refs. 1 and 2 that such an analysis leads to an expression for the total potential energy V of the loaded structure that is a function of the single displacement parameter C. Postbuckling equilibrium is then dependent on the simple criterion, $dV/dC = 0$. The resulting, postbuckling load-displacement relations are valid if the displacements from the unbuckled form are sufficiently small.

A1. Basic Potential Energy Expression

The total potential energy V of the loaded shell is the sum of the strain energy U and the potential energy of the external forces, Ω. In nondimensional notation,

$$\bar{V} = \bar{U} + \bar{\Omega} \tag{A3}$$

where $V = \left[2(1 - \nu^2)/(Etr^2)\right]V$, etc. In the Baruch-Singer formulation of the shell equations, the deformation geometry is expressed in terms of simplified Donnell-type kinematic relations. For such relations, the strain energy expression can be written

$$\bar{U} = \int_0^{2\pi} \int_0^{L/R} \left[\alpha_3 \epsilon_x^2 + \alpha_4 \epsilon_y^2 + 2\nu \epsilon_x \epsilon_y + \frac{1 - \nu}{2} \gamma_{xy}^2 + 2\alpha_1 \epsilon_x \kappa_x \right.$$

$$\left. + 2\alpha_2 \epsilon_y \kappa_y + \alpha_5 \kappa_x^2 + \alpha_6 \kappa_y^2 + 2\nu\gamma^2 \kappa_x \kappa_y + (\alpha_7 - 2\nu\gamma^2)\kappa_{xy}^2 \right] dx\, dy \tag{A4}$$

where

$$\epsilon_x = e_x + \frac{1}{2}\omega_y^2$$

$$\epsilon_y = e_y + \frac{1}{2}\omega_x^2 \qquad \text{(A5)}$$

$$\gamma_{xy} = e_{xy} + \omega_x\omega_y$$

and

$$e_x = u_{,x} \qquad \omega_x = -w_{,y} \qquad \kappa_x = -w_{,xx}$$

$$e_y = v_{,y} + w \qquad \omega_y = -w_{,x} \qquad \kappa_y = -w_{,yy} \qquad \text{(A6)}$$

$$e_{xy} = u_{,y} + v_{,x} \qquad \kappa_{xy} = -w_{,xy}$$

Equations (A4) - (A6) are the same as corresponding equations in an unpublished Lockheed work by E. V. Pittner.

In the Donnell-type formulation, the $\bar{\Omega}$ term is only a linear functional of the displacement components. Therefore it makes no direct contribution to the potential energy increment in Eq. (A8) below.

A2. Potential Energy Increment

To examine the equilibrium of the shell in a slightly buckled form, let

$$u = u_0 + \bar{u}\,, \quad v = v_0 + \bar{v}\,, \quad w = w_0 + \bar{w} \qquad \text{(A7)}$$

where $(u_0\,,\ v_0\,,\ w_0)$ represents an unbuckled equilibrium configuration corresponding to an applied load in the neighborhood of the critical load, and $(\bar{u}\,,\ \bar{v}\,,\ \bar{w})$ denotes a small finite additional displacement to a

nearby, buckled, equilibrium form at the same load. The change in potential energy corresponding to the additional displacement may be written

$$\Delta\bar{V} = \frac{1}{2}\,\delta^2\,\bar{V} + \frac{1}{3!}\,\delta^3\,\bar{V} + \frac{1}{4!}\,\delta^4\,\bar{V} \tag{A8}$$

where the three terms on the right represent the quadratic, cubic, and quartic terms, respectively, in $(\bar{u}\ ,\ \bar{v}\ ,\ \bar{w})$. The linear terms are missing by virtue of the principle of stationary potential energy. Then, from Eqs. (A3) - (A6):

$$\begin{aligned}\frac{1}{2}\,\delta^2\,\bar{V} = \int_0^{2\pi}\int_0^{L/R} \Big\{ & \Big[\alpha_3\bar{u}_{,x}^2 + \alpha_4(\bar{v}_{,y} + \bar{w})^2 + 2\nu\bar{u}_{,x}(\bar{v}_{,y} + \bar{w}) \\ & + \frac{1-\nu}{2}(\bar{u}_{,y} + \bar{v}_{,x})^2 - 2\alpha_1\bar{u}_{,x}\bar{w}_{,xx} - 2\alpha_2(\bar{v}_{,y} + \bar{w})\bar{w}_{,yy} + \alpha_5\bar{w}_{,xx}^2 \\ & + \alpha_6\bar{w}_{,yy}^2 + 2\nu\gamma^2\bar{w}_{,xx}\bar{w}_{,yy} + (\alpha_7 - 2\nu\gamma^2)\bar{w}_{,xy}^2\Big] \\ & + \Big[(\alpha_3 u_{0,x} + \nu w_0 - \alpha_1 w_{0,xx})\bar{w}_{,x}^2 + (\alpha_4 w_0 + \nu u_{0,x} - \alpha_2 w_{0,yy})\bar{w}_{,y}^2 \\ & + (1-\nu)(u_{0,y} + v_{0,x})\bar{w}_{,x}\bar{w}_{,y}\Big]\Big\}\,dx\,dy\end{aligned} \tag{A9}$$

$$\begin{aligned}\frac{1}{6}\,\delta^3\,\bar{V} = \int_0^{2\pi}\int_0^{L/R} \Big\{ & \alpha_3\bar{u}_{,x}\bar{w}_{,x}^2 + \alpha_4(\bar{v}_{,y} + \bar{w})\bar{w}_{,y}^2 - \alpha_1\bar{w}_{,xx}\bar{w}_{,x}^2 - \alpha_2\bar{w}_{,yy}\bar{w}_{,y}^2 \\ & + \nu\left[\bar{u}_{,x}\bar{w}_{,y}^2 + (\bar{v}_{,y} + \bar{w})\bar{w}_{,x}^2\right] + (1-\nu)\left[\bar{u}_{,y} + \bar{v}_{,x}\right]\bar{w}_{,x}\bar{w}_{,y}\Big\}\,dx\,dy\end{aligned} \tag{A10}$$

$$\frac{1}{24}\,\delta^4\,\bar{V} = \frac{1}{4}\int_0^{2\pi}\int_0^{L/R}\left\{\alpha_3\bar{w}_{,x}^4 + 2\bar{w}_{,x}^2\bar{w}_{,y}^2 + \alpha_4\bar{w}_{,y}^4\right\}dx\,dy \tag{A11}$$

where terms representing prebuckling rotations ω_{x0} and ω_{y0} have been neglected.

The terms containing the quantities u_0 , v_0 , w_0 are determined from an examination of prebuckling equilibrium. The analysis yields the relations:

$$\begin{aligned} \alpha_3 u_{0,x} + \nu w_0 - \alpha_1 w_{0,xx} &= \lambda_x \\ \alpha_4 w_0 + \nu u_{0,x} - \alpha_2 w_{0,yy} &= \lambda_y \\ \frac{1-\nu}{2}(u_{0,y} + v_{0,x}) &= \lambda_{xy} \end{aligned} \tag{A12}$$

where

$$\begin{aligned} \lambda_x &= \frac{1-\nu^2}{Et} N_{x0} \\ \lambda_y &= \frac{1-\nu^2}{Et} N_{y0} \\ \lambda_{xy} &= \frac{1-\nu^2}{Et} N_{xy0} \end{aligned} \tag{A13}$$

and N_{x0} is membrane force (lb/in), etc.; if P_x is total axial load, $N_{x0} = P_x/(2\pi R)$. These are the same as Eqs. (5) of Ref. 7. The subsequent analysis is restricted to axial compression loading only. Accordingly, $\lambda_y = \lambda_{xy} = 0$.

The incremental displacement ($\bar{u}$, $\bar{v}$, $\bar{w}$) may be expressed in terms of the buckle form plus a small perturbation, as follows:

$$\bar{u} = Cu_1 + u_2 \quad , \quad \bar{v} = Cv_1 + v_2 \quad , \quad \bar{w} = Cw_1 + w_2 \tag{A14}$$

where (u_1 , v_1 , w_1) is the buckle mode, C is amplitude of the buckle mode, (u_2 , v_2 , w_2) is in some sense orthogonal to (u_1 , v_1 , w_1), and the perturbation is much smaller than the buckle mode displacement. In terms of (u_1 , v_1 , w_1) and (u_2 , v_2 , w_2), the potential energy increment is of the form

$$\Delta\bar{V} = \psi_1 + \psi_2 \tag{A15}$$

where

$$\psi_1 = \left\{P_2^0\left[u_1\right] + \lambda_x P_2^1\left[u_1\right]\right\} C^2 + P_3\left[u_1\right] C^3 + P_4\left[u_1\right] C^4 \tag{A16}$$

and

$$\psi_2 = \left\{P_2^0\left[u_2\right] + \lambda_x P_2^1\left[u_2\right]\right\} + P_{21}\left[u_1, u_2\right] C^2 + \ldots \tag{A17}$$

and terms that are not explicitly included may be omitted because of the orthogonality condition and the smallness of (u_2 , v_2 , w_2). From Eqs. (A9) - (A11):

$$\left\{P_2^0\left[u_1\right] + \lambda_x P_2^1\left[u_1\right] = (\lambda_x - \lambda_{CL}) \int_0^{2\pi} \int_0^{L/R} w_{1,x}^2 \, dx \, dy\right.$$

$$\begin{aligned} P_3\left[u_1\right] = \int_0^{2\pi} \int_0^{L/R} & \alpha_3 u_{1,x} w_{1,x}^2 + \alpha_4 (v_{1,y} + w_1) w_{1,y}^2 \\ & - \alpha_1 w_{1,xx} w_{1,x}^2 - \alpha_2 w_{1,yy} w_{1,y}^2 \\ & + \upsilon\left[u_{1,x} w_{1,y}^2 + (v_{1,y} + w_1) w_{1,y}^2\right] \\ & \left. + (1 - \upsilon)(u_{1,y} + v_{1,x}) w_{1,x} w_{1,y}\right] dx \, dy \end{aligned} \tag{A18}$$

$$P_4\left[u_1\right] = \int_0^{2\pi}\int_0^{L/R} \left[\frac{1}{4}\alpha_3 w_{1,x}^4 + \frac{1}{4}\alpha_4 w_{1,y}^4 + \frac{1}{2} w_{1,x}^2 w_{1,y}^2\right] dx\, dy \qquad \text{(A18 cont'd)}$$

where λ_{CL} is the classical critical value of λ_x. Similarly,

$$\begin{aligned} P_2^0\left[u_2\right] + \lambda_x P_2^1\left[u_2\right] = \int_0^{2\pi}\int_0^{L/R} \Big[&\alpha_3 u_{2,x}^2 + \alpha_4(v_{2,y} - w_2)^2 + 2\nu u_{2,x}(v_{2,y} - w_2) \\ &+ \frac{1-\nu}{2}(v_{2,x} + u_{2,y})^2 - 2\alpha_1 u_{2,x} w_{2,xx} \\ &- 2\alpha_2(v_{2,y} - w_2) w_{2,yy} + \alpha_5 w_{2,xx}^2 \\ &+ \alpha_6 w_{2,yy}^2 + 2\nu\gamma^2 w_{2,xx} w_{2,yy} \\ &+ (\alpha_7 - 2\nu\gamma^2) w_{2,xy}^2 + \lambda_x w_{2,x}^2\Big] dx\, dy \end{aligned} \qquad \text{(A19)}$$

$$\begin{aligned} P_{21}\left[u_1, u_2\right] = \int_0^{2\pi}\int_0^{L/R} \Big\{&\left[\alpha_3 w_{1,x}^2 + \nu w_{1,y}^2\right] u_{2,x} \\ &+ \left[(1-\nu) w_{1,x} w_{1,y}\right] u_{2,y} + \left[(1-\nu) w_{1,x} w_{1,y}\right] v_{2,x} \\ &+ \left[\alpha_4 w_{1,y}^2 + \nu w_{1,x}^2\right] v_{2,y} + \left[\alpha_4 w_{1,y}^2 + \nu w_{1,x}^2\right] w_2 \\ &+ \Big[2\alpha_3 u_{1,x} w_{1,x} - 2\alpha_1 w_{1,x} w_{1,xx} \\ &\quad + 2\nu(v_{1,y} + w_1) w_{1,x} + (1-\nu)(u_{1,y} + v_{1,x}) w_{1,y}\Big] w_{2,x} \\ &+ \Big[2\alpha_4(v_{1,y} + w_1) w_{1,y} - 2\alpha_2 w_{1,y} w_{1,yy} \\ &\quad + 2\nu u_{1,x} w_{1,y} + (1-\nu)(u_{1,y} + v_{1,x}) w_{1,x}\Big] w_{2,y} \\ &+ \left[-\alpha_1 w_{1,x}^2\right] w_{2,xx} + \left[-\alpha_2 w_{1,y}^2\right] w_{2,yy}\Big\} dx\, dy \end{aligned}$$

A3. Classical Stability Analysis

The buckle load and mode are readily determined from Eq. (A9) by use of the minimum potential energy theory of stability. According to the Trefftz criterion, the classical solution for the critical load is given by the Euler equations for the second-variation expression. For this purpose, let the applied load be the critical load itself instead of a load in the neighborhood of the critical load, and replace the incremental displacement ($\bar{u}$, $\bar{v}$, $\bar{w}$) in Eq. (A9) by (Cu_1 , Cv_1 , Cw_1). The Euler equations obtained by variation with respect to u_1 , v_1 , w_1 are then found to be:

$$\alpha_3 u_{1,xx} + \frac{1-\nu}{2} u_{1,yy} + \frac{1+\nu}{2} v_{1,xy} + \nu w_{1,x} - \alpha_1 w_{1,xxx} = 0$$

$$\frac{1+\nu}{2} u_{1,xy} + \frac{1-\nu}{2} v_{1,xx} + \alpha_4 (v_{1,yy} + w_{1,y}) - \alpha_2 w_{1,yyy} = 0$$

$$\alpha_5 w_{1,xxxx} + \alpha_7 w_{1,xxyy} + \alpha_6 w_{1,yyyy} - \alpha_1 u_{1,xxxx} - \alpha_2 (v_{,yyy} + 2w_{,yy}) + \alpha_4 (v_{1,y} + w_1) + \nu u_{1,x} - \lambda_{CL} w_{1,xx} = 0 \qquad \text{(A20)}$$

Equations (A20) are the same as Eqs. (12) of Ref. 7.

The present analysis is restricted to cylinders with simple-support edges. The simple-support boundary conditions are:

$$w_1 = w_{1,xx} = v_1 = u_{1,x} = 0 \quad \text{at} \quad x = 0, L/R \qquad \text{(A21)}$$

For these boundary conditions the solution to Eqs. (A20) is of the form

$$\begin{aligned} u_1 &= A \cos mx \sin ny \\ v_1 &= B \sin mx \cos ny \\ w_1 &= \sin mx \sin ny \end{aligned} \qquad \text{(A22)}$$

where A , B are constants, $m \equiv \bar{m}\pi R/L$, $\bar{m}$ is a positive integer, and $n = 2, 3, 4, \ldots$ for asymmetric buckling. Introduction into Eqs. (A20) yields the expression for the classical critical load given in Eq. (1). For axisymmetric buckling,

$$u_1 = A \cos mx$$

$$v_1 = 0 \qquad \text{(A23)}$$

$$w_1 = \sin mx$$

Introduction into Eqs. (A20) gives Eq. (3).

A4. Determination of (u_2 , v_2 , w_2) for Stationary $\Delta\bar{V}$

Equations (A17) and (A19) express the ψ_2 part of the potential energy increment as a functional of the displacement components u_2 , v_2 , w_2. The functions u_2 , v_2 , w_2 are determined from the requirement that, for fixed values of C, $\Delta\bar{V}$ must be stationary in these displacement components. Examination of the Euler equations obtained by variation of $\Delta\bar{V}$ with respect to u_2 , v_2 , w_2 shows the functions to be of the form

$$u_2 = U_0(x) + U_1(x) \cos 2ny$$

$$v_2 = V_1(x) \sin 2ny \qquad \text{(A24)}$$

$$w_2 = W_0(x) + W_1(x) \cos 2ny$$

Introduction into Eq. (A19) and integration yield the expressions given in Eq. (9).

Both ψ_1 and ψ_2 depend on λ_x as a parameter. However, Koiter has shown (Ref. 2, 3) that, for small values of the displacement amplitude C, λ_x may be approximated by λ_{CL} in the expression for ψ_2. Equation (A17) may then be written

$$\psi_2 = \left\{ P_2^0 \left[u_2\right] + \lambda_{CL} P_2^1 \left[u_2\right] \right\} + P_{21}\left[u_1, u_2\right] C^2 \qquad (A25)$$

The equations for stationary ψ_2 (or $\Delta\bar{V}$) are nonhomogeneous linear equations in the displacement variables, whose right sides are proportional to C^2. Thus, each of the displacement variables itself is proportional to C^2, and ψ_2 is proportional to C^4. Accordingly, the value of ψ_2 that corresponds to stationary $\Delta\bar{V}$ may be written in the form shown in Eq. (10). For ψ_1, introduction of Eqs. (A22) into Eqs. (A16) and (A18) and integration yield

$$\psi_1 = \frac{\pi L}{2R}\left[(\lambda_x - \lambda_{CL})m^2C^2 + \frac{1}{64}\left(9\alpha_3 m^4 + 2m^2n^2 + 9\alpha_4 n^4\right)\right] C^4 \qquad (A26)$$

Thus, for a fixed value of C, Eqs. (10) and (A26) give for stationary $\Delta\bar{V}$ the expression

$$\Delta\bar{V} = \frac{\pi L}{2R}\left\{\left[(\lambda_x - \lambda_{CL})m^2\right] C^2 + \frac{1}{2}\left[\frac{1}{32}\left(9\alpha_3 m^4 + 2m^2n^2 + 9\alpha_4 n^4\right) + \frac{2R}{\pi L} P\right] C^4\right\} \qquad (A27)$$

Let

$$S \equiv \frac{1}{m^2 \lambda_{CL}}\left[\frac{1}{32}\left(9\alpha_3 m^4 + 2m^2n^2 + 9\alpha_4 n^4\right) + \frac{2R}{\pi L} P\right] \qquad (A28)$$

Then

$$\Delta\bar{V} = \frac{\pi L}{2R} m^2 \left[(\lambda_x - \lambda_{CL})C^2 + \left(\frac{1}{2} S\lambda_{CL}\right)C^4\right] \qquad (A29)$$

Equation (A29) expresses the potential energy increment in terms of the single parameter C. For equilibrium, $d(\Delta\bar{V})/dC = 0$. Consequently,

$$C^2 = \frac{1 - \lambda_x/\lambda_{CL}}{S} \tag{A30}$$

Equation (A30) can be re-written as shown in Eq. (5).

A5. Numerical Analysis

Finite differences and numerical integration were used to determine the displacement variables U_0, W_0, U_1, V_1, W_1 for stationary Ψ_2. From Eqs. (8) and (9), Ψ_2 is of the form

$$\Psi_2 = \int_0^{L/R} F(U_0', W_0, U_1, V_1, W_1)dx \tag{A31}$$

(U_0, as distinguished from U_0', does not explicitly appear). Let $(U_0')_0 = X_0$, $(W_0)_0 = X_1$, $(U_1)_0 = X_2$, $(V_1)_0 = X_3$, $(W_1)_0 = X_4$, $(U_0')_1 = X_5$, $(W_0)_1 = X_6$, etc. Then Eq. (A31) can be approximated by the relation

$$\Psi_2 = \sum_{i=0}^{5(N+1)} F(X_i)h \tag{A32}$$

where $(N+1)$ is the number of stations in the interval $0 \le x \le L/R$, hR is the constant distance between stations, and $Nh = L/R$. Forward and backward differences were used at the ends to avoid use of fictitious points outside the interval.

For stationary ψ_2 , $\partial\psi_2/\partial X_j = 0$. Therefore

$$\sum_{i=0}^{5(N+1)} \frac{\partial F_i}{\partial X_j} = 0 \; ; \qquad j = 0 \, , \, 1 \, , \, 2 \, , \, \ldots \, , \, 5(N+1) \tag{A33}$$

Equation (A33) gives a set of $5(N+1)$ nonhomogeneous linear equations in the X_i . Solution of the equations gives values of the X_i for stationary ψ_2 . Introduction of these X_i into Eq. (A32) yields P , Eq. (10).

The kinematic boundary conditions for the numerical analysis are

$$W_0 = V_1 = W_1 = 0 \quad \text{at} \quad x = 0 \, , \, L/R \tag{A34}$$

Hence the number of simultaneous equations is $(5N - 1)$. The calculations are shortened by the fact that the variables U_0' , W_0 and the variables U_1 , V_1 , W_1 appear as two uncoupled sets in the numerical analysis.

Calculations were carried out on the Univac 1108 computer. With double-precision arithmetic, 41 finite difference stations were found to be sufficient for at least two-significant-figure accuracy in the calculation of the sensitivity parameter S . Except where noted, Poisson's ratio was taken to be 0.3 in all numerical work.

A6. Initially Imperfect Cylinders

Koiter has shown that the analysis may be modified to provide an approximate equation for the load-displacement curve of an initially imperfect cylinder, as follows. Let $w^* = w^*(x,y)$ represent a small initial

deviation from a true cylindrical form. Then the strain-displacement relations in Eqs. (A5) and (A6) are replaced by the expressions

$$\begin{aligned} \epsilon_x &= u_{,x} + \frac{1}{2} w_{,x}^2 + w^*_{,x} w_{,x} \\ \epsilon_y &= v_{,y} + w + \frac{1}{2} w_{,y}^2 + w^*_{,y} w_{,y} \\ \gamma_{xy} &= u_{,y} + v_{,x} + w_{,x} w_{,y} + w^*_{,x} w_{,y} + w^*_{,y} w_{,x} \end{aligned} \tag{A35}$$

where w represents displacement from the slightly non-cylindrical initial configuration.

Introduction of Eqs. (A35) into the potential energy expression in place of the previous strain-displacement relations, replacement of u by $(u_0 + Cu_1 + u_2)$, etc., neglect of prebuckling rotations ω_{x0}, ω_{y0}, and retention of only the largest term in the displacement components yields the following additional term which must be included in the expression for the potential energy increment in Eqs. (A15) - (A19):

$$\Delta\bar{V}^* = 2\lambda_x C \int_0^{2\pi} \int_0^{L/R} w^*_{,x} w_{1,x} \, dx \, dy \tag{A36}$$

Integration by parts and introduction of the requirement that w^* be zero on $x = 0, L/R$ gives

$$\Delta\bar{V}^* = -2\lambda_x C \int_0^{2\pi} \int_0^{L/R} w^* w_{1,xx} \, dx \, dy \tag{A37}$$

For simplicity, we assume the initial imperfection to be of the form of the buckle mode, i.e., we let

$$w^* = C^* \sin mx \sin ny \tag{A38}$$

where C^* is amplitude of imperfection as a fraction of cylinder radius R. Introduction of Eq. (A38) and the expression for w_1 from Eq. (A22), and integration, yield

$$\Delta\bar{V}^* = \frac{\pi L}{2R} m^2 (2\lambda_x C^*) C \tag{A39}$$

Addition of this term to the expression for the potential energy increment in Eq. (A29) gives

$$\Delta\bar{V} = \frac{\pi L}{2R} m^2 \left[(\lambda_x - \lambda_{CL}) C^2 + (\tfrac{1}{2} S\lambda_{CL}) C^4 + (2\lambda_x C^*) C \right] \tag{A40}$$

For equilibrium, $d(\Delta\bar{V})/dC = 0$. Therefore the approximate relation for the equilibrium path of the imperfect cylinder is

$$SC^3 + \left(\frac{\lambda_x}{\lambda_{CL}} - 1\right) C + \frac{\lambda_x}{\lambda_{CL}} C^* = 0 \tag{A41}$$

Equation (A41) can be re-written in the form given in Eq. (12)

The maximum point λ_M on the equilibrium path of an imperfection-sensitive cylinder ($S > 0$) is determined by the relation $d\lambda_x/dC = 0$. From Eq. (A41) we obtain

$$\left(1 - \frac{\lambda_M}{\lambda_{CL}}\right)^{3/2} = \frac{3\sqrt{3}}{2} \frac{\lambda_M}{\lambda_{CL}} \sqrt{S} \; |C^*| \quad , \; S > 0 \; . \tag{A42}$$

REFERENCES

1. W. T. Koiter, "On the Stability of Elastic Equilibrium" (in Dutch with English summary). Thesis, Delft, H. J. Paris, Amsterdam, 1945.

2. W. T. Koiter, "Elastic Stability and Postbuckling Behavior," Proc. Symp. Nonlinear Problems, edited by R. E. Langer, University of Wisconsin Press, pp 257-275, 1963.

3. W. T. Koiter, "Buckling and Post-Buckling Behavior of a Cylindrical Panel under Axial Compression," National Aeronautical Research Institute, Amsterdam, Report S. 476, May 1956.

4. B. Budiansky and J. W. Hutchinson, "A Survey of Some Buckling Problems," AIAA Journal, Sept. 1966, pp 1505-1510.

5. J. W. Hutchinson and J. C. Amazigo, "Imperfection-Sensitivity of Eccentrically Stiffened Cylindrical Shells," AIAA Journal, March 1967, pp 392-401.

6. W. T. Koiter, "The Effect of Axisymmetric Imperfections on the Buckling of Cylindrical Shells under Axial Compression," Koninkl. Nederl. Akademie van Wetenschappen, Amsterdam, 1963.

7. M. Baruch and J. Singer, "Effect of Eccentricity of Stiffeners on the General Instability of Stiffened Cylindrical Shells under Hydrostatic Pressure," Jour. Mech. Engr. Sci., Vol. 5, No. 1, 1963, pp 23-27.

8. J. Singer, M. Baruch, and O. Harari, "On the Stability of Eccentrically Stiffened Cylindrical Shells under Axial Compression," Int. J. Solids Structures, Vol. 3, 1967, pp 445-470.

9. M. F. Card, and R. Jones, "Compressive Buckling of Cylinders with Eccentric Longitudinal Stiffness," NASA Langley Research Center TN-D 3639, Oct 1966.

10. R. Milligan, G. Gerard, C. Lakshmikanthan, and H. Becker, "General Instability of Orthotropically Stiffened Cylinders. Part I - Axial Compression, Torsion, and Hydrostatic Pressure Loadings," AFFDL TR 65 161, Air Force Flight Dynamics Lab., Wright Patterson Air Force Base, July 1965.

11. J. P. Peterson, and M. B. Dow, "Compression Tests on Circular Cylinders Stiffened Longitudinally by Closely Spaced Z-Section Stringers," NASA Memo 2-12-59L, March 1959.

12. L. Katz, "Compression Tests on Integrally Stiffened Cylinders." NASA TM X-53315, George C. Marshall Space Flight Center, August 1965.

13. B. O. Almroth, D. Bushnell, and L. H. Sobel, "Buckling of Shells of Revolution with Various Wall Constructions," Lockheed Missiles and Space Co., Report 4-17-67-1, June 1967.

TABLE 1 - Influence of Stringer Torsional Stiffness

Cyl. No.	R/t	L/R	α_1	α_3	α_5	α_6	α_7	λ_{CL}	$\bar{m}$, n	S	
1.	338	3.98	.01597	1.926	$.355\times10^{-3}$	$.729\times10^{-6}$	1.390×10^{-5}	.00355	1, 6	724.	torsional stiffness included
							$.1458\times10^{-5}$	.00310	1, 6	789.	torsional stiffness neglected
								-13.		9.	percent error
2.	345	3.98	-.01648	1.954	$.363\times10^{-3}$	$.699\times10^{-6}$	1.419×10^{-5}	.00219	1, 5	596.	torsional stiffness included
							$.1398\times10^{-5}$	.00178	2, 7	1270.	torsional stiffness neglected
								-19.		113.	percent error
3.	347	2.49	.01653	1.964	$.369\times10^{-3}$	$.691\times10^{-6}$	1.429×10^{-5}	.00427	1, 7	1570.	torsional stiffness included
							$.1382\times10^{-5}$	.00364	1, 7	1790.	torsional stiffness neglected
								-15.		14.	percent error
4.	341	2.49	-.01632	1.945	$.362\times10^{-3}$	$.716\times10^{-6}$	1.408×10^{-5}	.00231	1, 6	1080.	torsional stiffness included
							$.1432\times10^{-5}$	.00184	1, 7	977.	torsional stiffness neglected
								-20.		-9.	percent error

$\alpha_2 = 0$, $\alpha_4 = 1$, $\nu = 0.32$

TABLE 2 - Test Data for Stringer Stiffened Cylinders

Card and Jones, Ref. 9
($\alpha_2 = 0$, $\alpha_4 = 1$)

Cyl. No.	R/t	L/R	α_1	α_3	α_5	α_6	α_7	$-\lambda_{CL}$	S	$\frac{\lambda_{exp}}{\lambda_{CL}}$
					$\times 10^{-3}$	$\times 10^{-6}$	$\times 10^{-5}$	$\times 10^{-2}$	$\times 10^{4}$	
1*	338	3.98	.01597	1.926	.355	.729	1.390	.359	.07	1.64
2*	345	3.98	-.01648	1.954	.363	.699	1.419	.223	.06	1.16
3*	347	2.49	.01653	1.964	.369	.691	1.429	.430	.16	1.60
4*	341	2.49	-.01632	1.945	.362	.716	1.408	.233	.11	1.34
5	389	3.71	.01206	1.759	.318	.531	.1657	.253	.09	1.42
6	397	3.71	-.01206	1.759	.318	.531	.1657	.165	.07	1.30
7	407	2.62	.01202	1.759	.315	.527	.1643	.291	.17	1.45
8	397	2.62	-.01202	1.759	.315	.527	.1643	.166	.10	1.63
9	407	1.864	.01206	1.755	.319	.541	.1678	.361	.27	1.74
10	396	1.864	-.01206	1.755	.319	.541	.1678	.183	.10	2.04
11	404	1.305	.01212	1.759	.321	.537	.1672	.472	.41	1.82
12	397	1.305	-.01212	1.759	.321	.537	.1672	.230	.05	2.66

* These four cylinders also appear in Table 1. For these, ν was taken to be 0.32 in . to match the data in Table 3 of Ref. 8. For Nos. 5 - 12, 0.30 was used for ν.

Milligan, Gerard, Lakshmikanthan, and Becker, Ref. 10
($\alpha_1 = \alpha_2 = 0$, $\nu = 0.3$)

Cyl. No.	R/t	L/R	α_3	α_4	α_5	α_6	α_7	$-\lambda_{CL}$	S	$\frac{\lambda_{exp}}{\lambda_{CL}}$
					$\times 10^{-5}$	$\times 10^{-5}$	$\times 10^{-5}$	$\times 10^{-2}$	$\times 10^{4}$	
13	362	.521	1.326	1.242	.1999	.1046	.2450	.221	2.58	.72
14	365	.524	1.359	1.260	.2186	.1047	.2642	.226	2.50	.79
15	317	.526	1.176	1.148	.1530	.1186	.2020	.210	8.90	.82
16	286	.534	1.140	1.121	.1647	.1385	.2213	.221	8.37	.82
22	655	1.052	1.800	1.437	.2316	.0370	.2505	.172	1.23	.89
23	692	.789	1.935	1.475	.2798	.0337	.2987	.183	2.04	.86
24	380	1.052	1.393	1.278	.2264	.0986	.2698	.225	2.52	.82
25	380	.789	1.166	1.140	.1024	.0813	.1359	.173	11.83	.84

TABLE 2 (Continued)

Milligan, Gerard, Lakshmikanthan, and Becker, Ref. 10 (Continued)
($\alpha_1 = \alpha_2 = 0$, $\nu = 0.3$)

Cyl. No.	R/t	L/R	α_3	α_4	α_5	α_6	α_7	$-\lambda_{CL}$	S	$\frac{\lambda_{exp}}{\lambda_{CL}}$
					$\times 10^{-5}$	$\times 10^{-5}$	$\times 10^{-5}$	$\times 10^{-2}$	$\times 10^{4}$	
26	349	.524	1.351	1.256	.2344	.1145	.2842	.235	2.39	.86
27	322	.797	1.346	1.252	.2697	.1337	.3278	.253	1.04	.72
28	604	.526	1.760	1.425	.2492	.0434	.2709	.194	3.41	.86
31	294	1.052	1.145	1.124	.1574	.1311	.2111	.216	8.58	.74
36	281	.789	1.135	1.129	.1679	.1405	.2251	.223	8.53	.76
38	314	.787	1.200	1.164	.1696	.1241	.2211	.219	8.47	.78
41	314	.889	1.329	1.243	.2679	.1391	.3280	.256	2.91	.86
43	613	.917	1.850	1.500	.3168	.0408	.3338	.193	1.42	1.13

Peterson and Dow, Ref. 11
($\alpha_2 = 0$, $\alpha_4 = 1$)

Cyl. No.	R/t	L/R	α_1	α_3	α_5	α_6	α_7	$-\lambda_{CL}$	S	$\frac{\lambda_{exp}}{\lambda_{CL}}$
			$\times 10^{-2}$		$\times 10^{-3}$	$\times 10^{-6}$	$\times 10^{-6}$	$\times 10^{-2}$	$\times 10^{4}$	
1	602	1.070	-.764	1.781	.1438	.230	.730	.158	.14	2.50
2	602	0.813	-.764	1.781	.1438	.230	.730	.217	.05	2.80

Katz, Ref. 12
($\alpha_2 = 0$, $\alpha_4 = 1$)

Cyl. No.	R/t	L/R	α_1	α_3	α_5	α_6	α_7	$-\lambda_{CL}$	S	$\frac{\lambda_{exp}}{\lambda_{CL}}$
			$\times 10^{-2}$		$\times 10^{-5}$	$\times 10^{-6}$	$\times 10^{-6}$	$\times 10^{-2}$	$\times 10^{4}$	
5A-1	697	2.12	.1080	1.225	.659	.1716	.822	.100	.44	0.62
5A-2	699	2.11	.1080	1.225	.659	.1716	.822	.100	.44	0.59
5B-1	694	2.13	.1532	1.320	.927	.1716	1.022	.107	.45	0.57
5C-1	694	2.13	.252	1.465	1.670	.1716	.200	.111	.50	0.75
5C-2	694	2.13	.252	1.465	1.670	.1716	.200	.111	.50	0.89

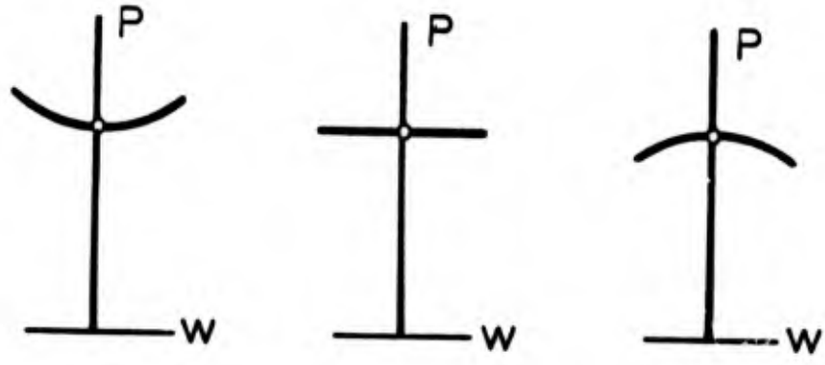

Fig. 1 Load-Displacement Curves for Perfect Structures

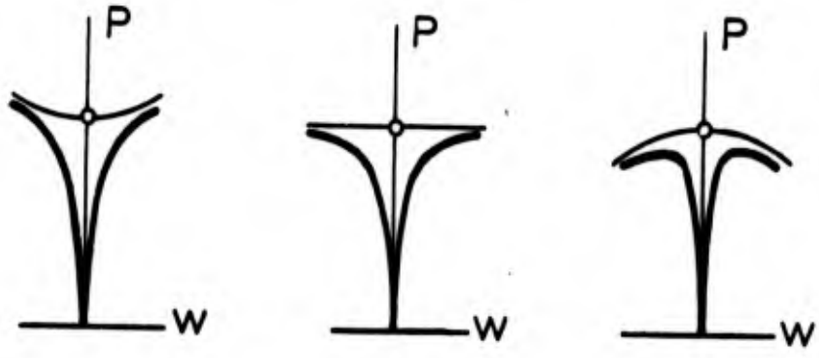

Fig. 2 Load-Displacement Curves for Imperfect Structures

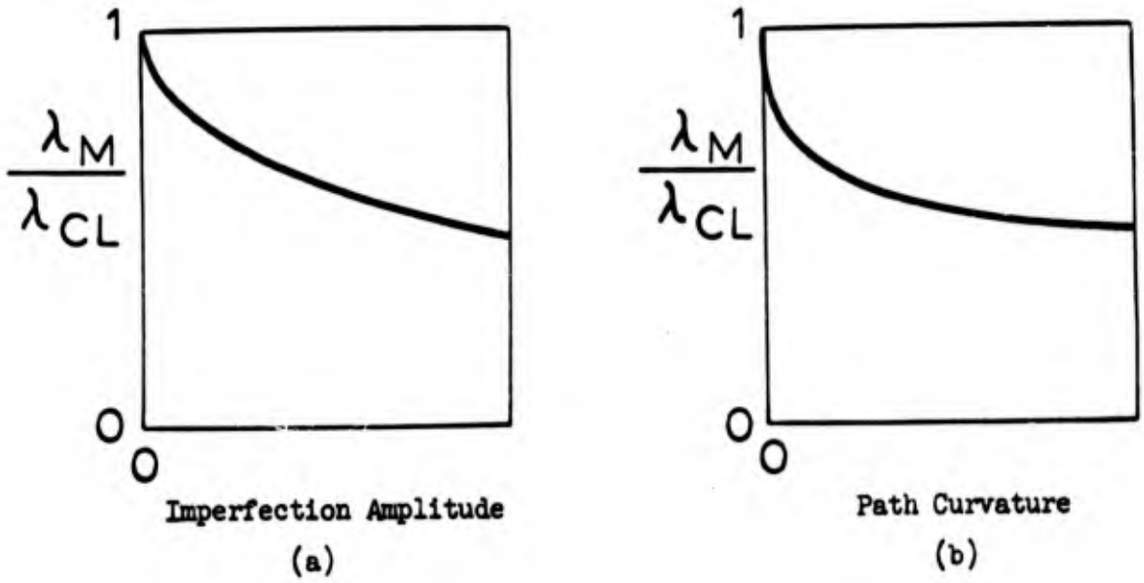

Fig. 3 Influence of Imperfection Amplitude and Path Curvature

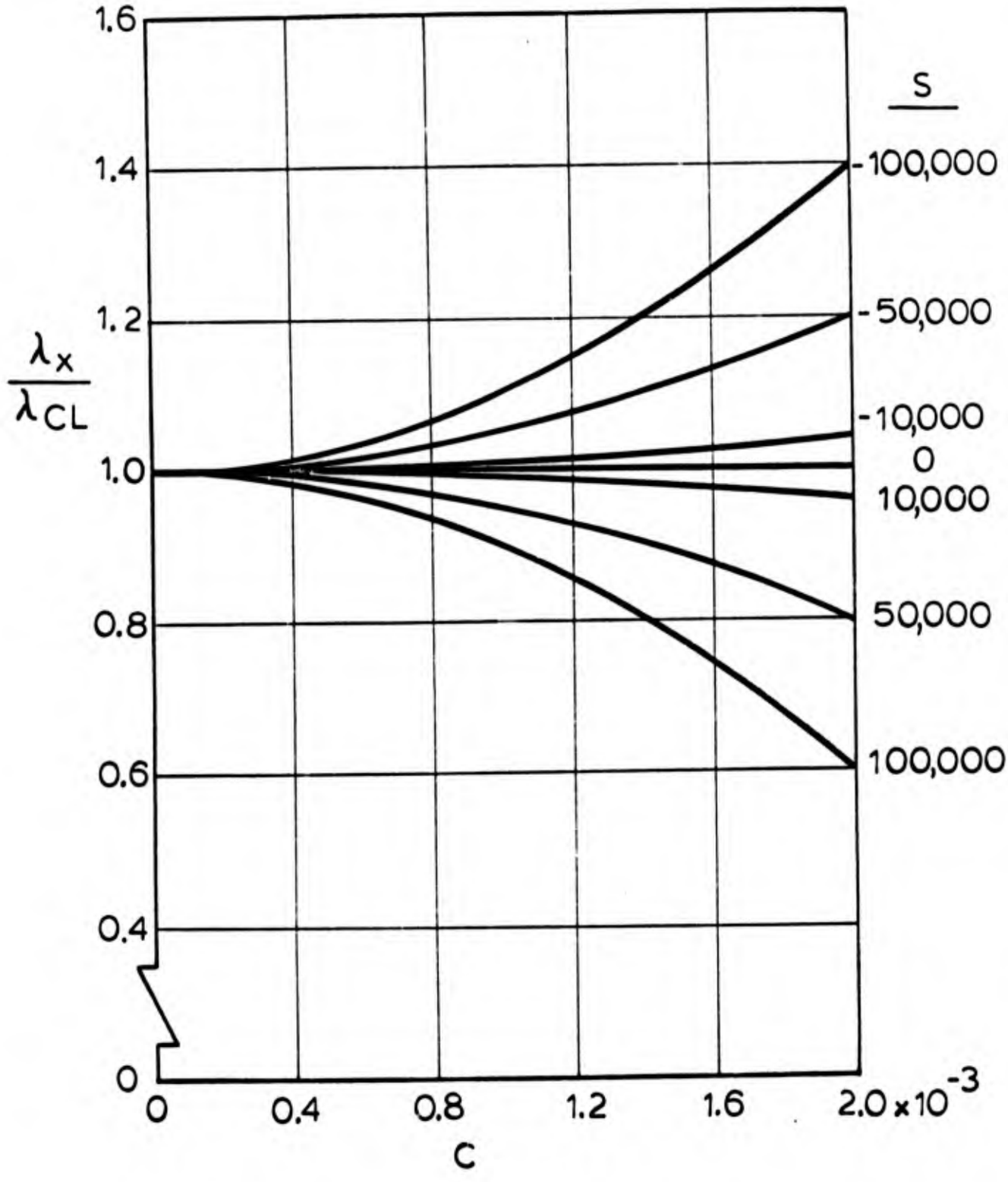

Fig. 4 Influence of Sensitivity Parameter S on Load-Displacement Curves

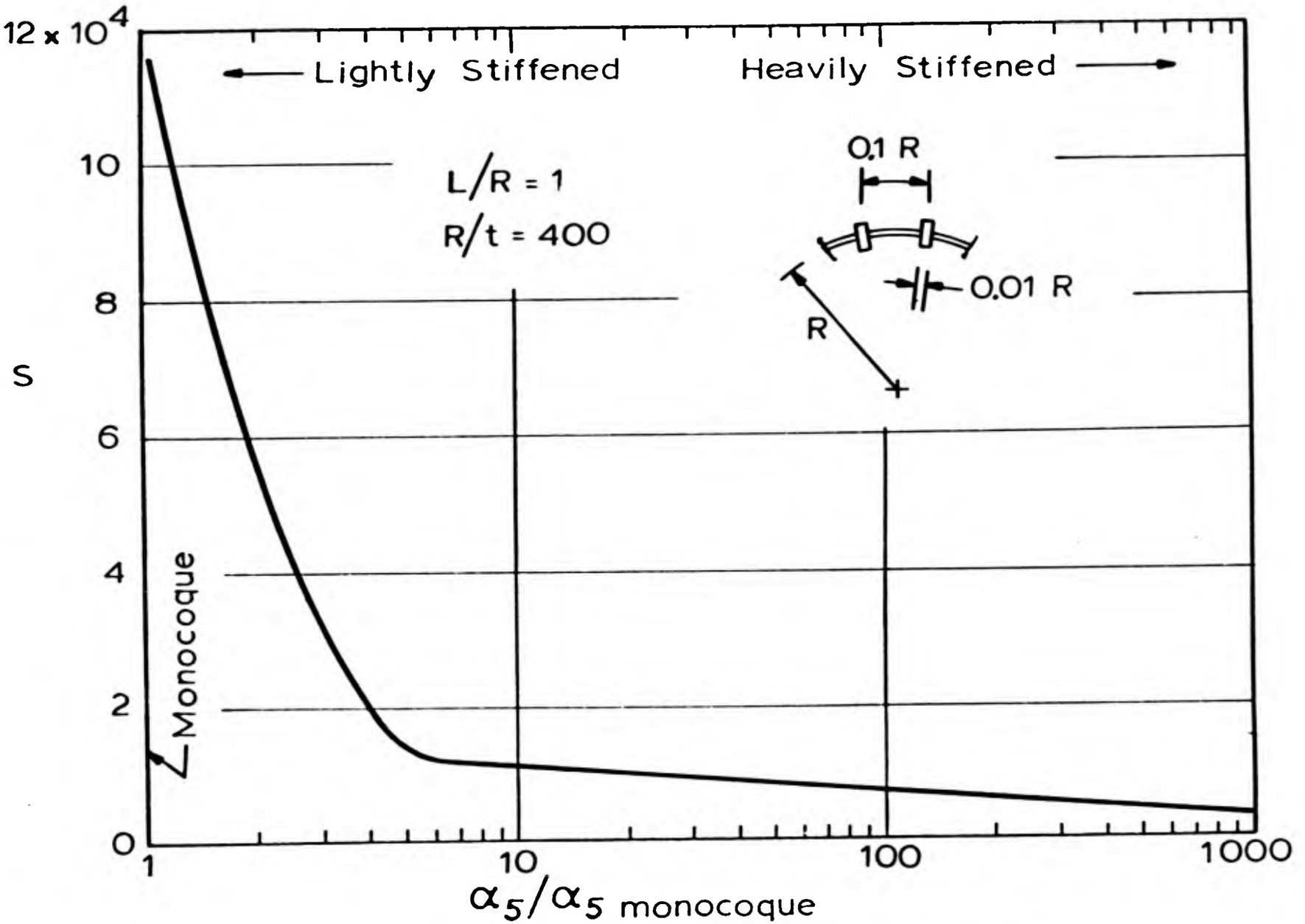

Fig. 5 Imperfection Sensitivity as a Function of Stringer Bending Stiffness

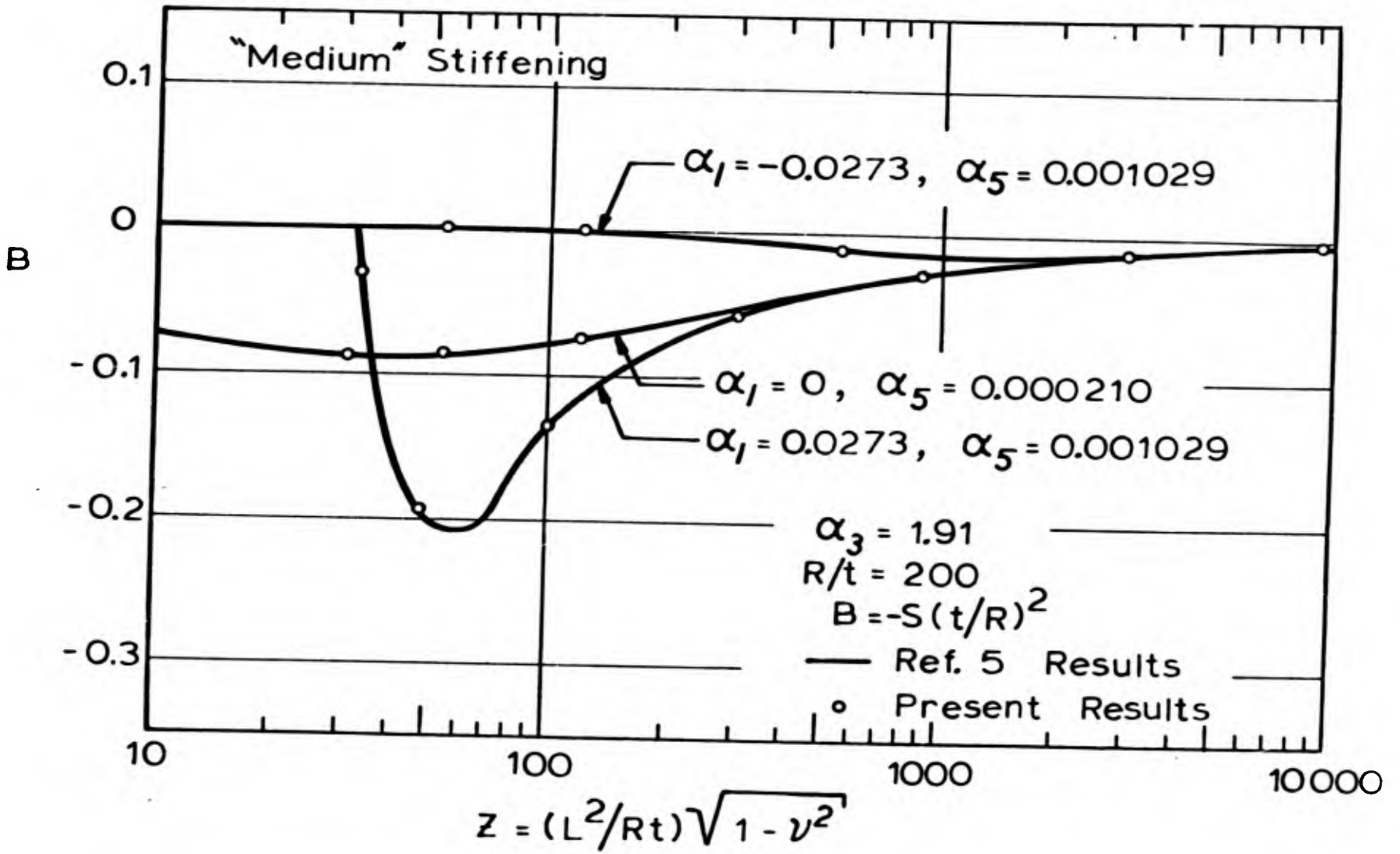

Fig. 6 Comparison with Results from Ref. 5

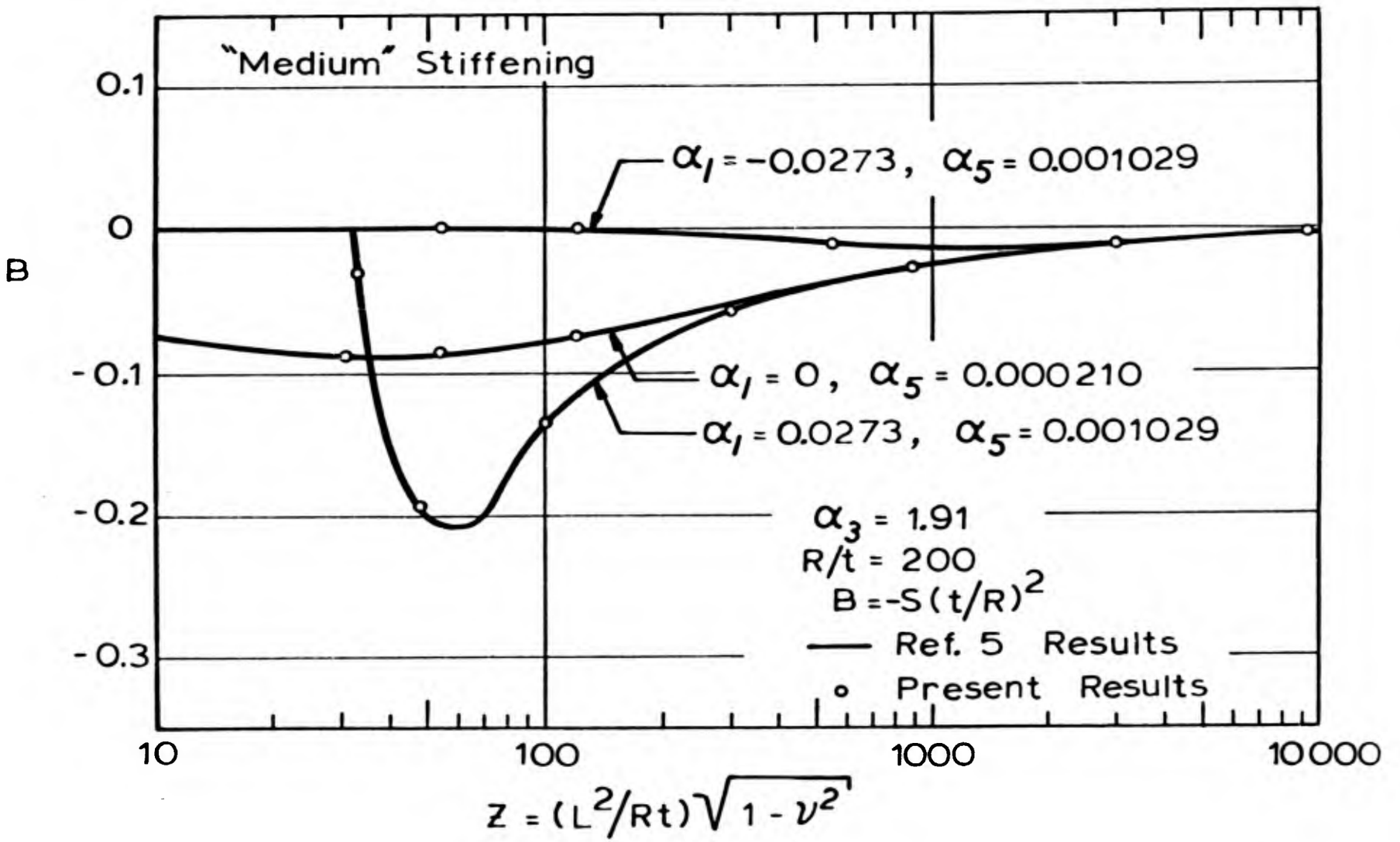

Fig. 6 Comparison with Results from Ref. 5

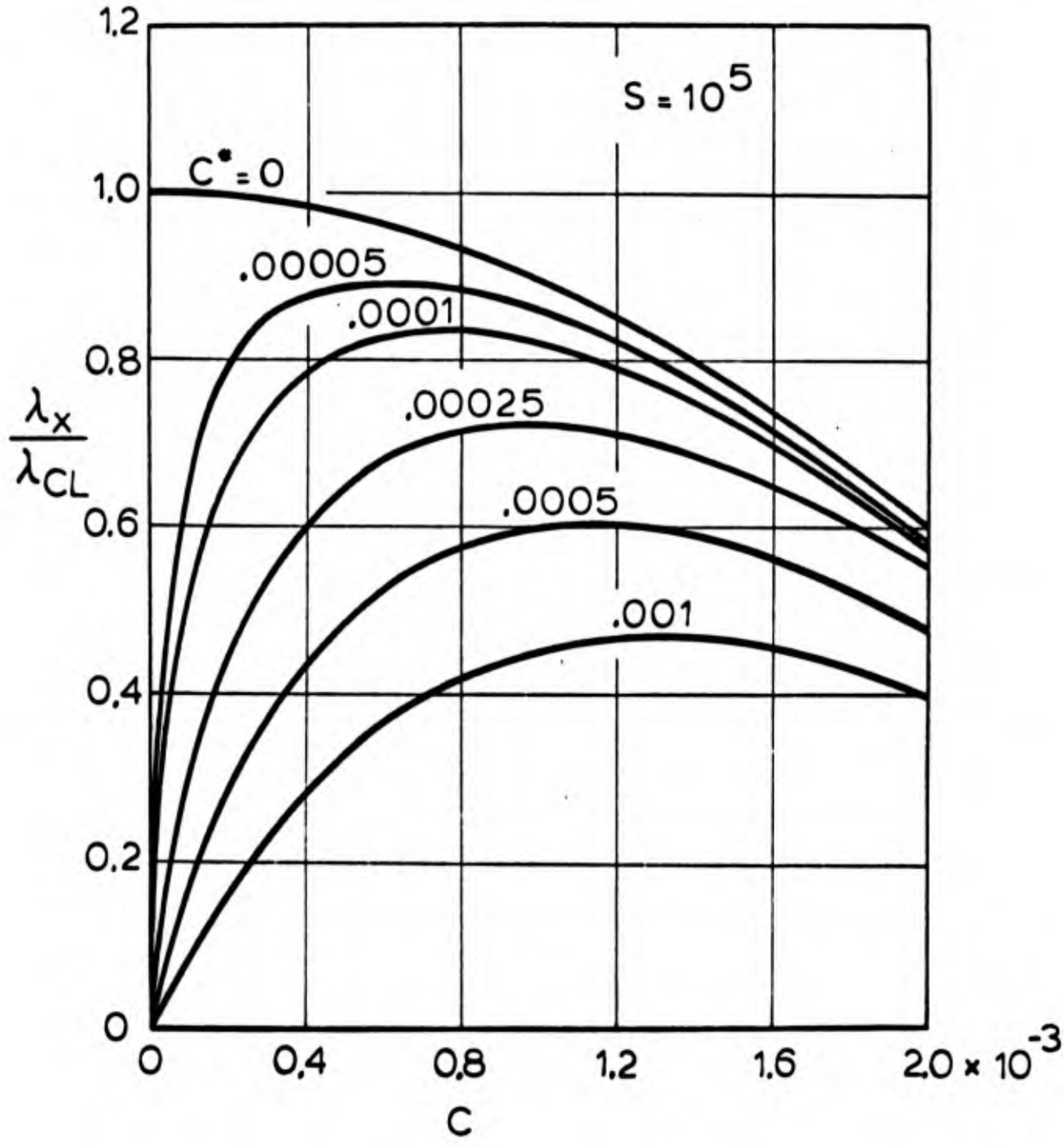

Fig. 7 Influence of Imperfection Amplitude on Load-Displacement Curves

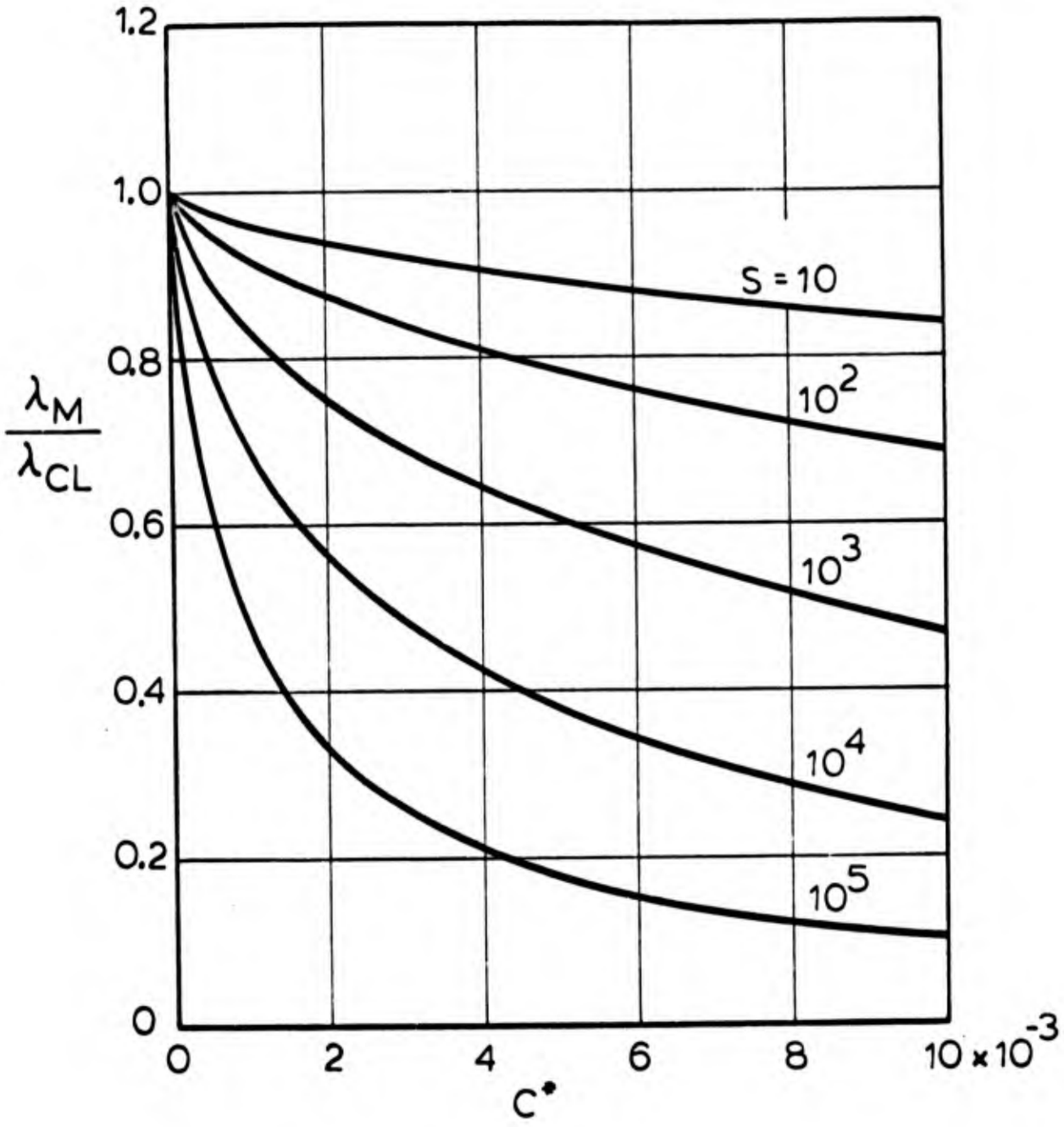

Fig. 8 Critical Load vs Imperfection Amplitude

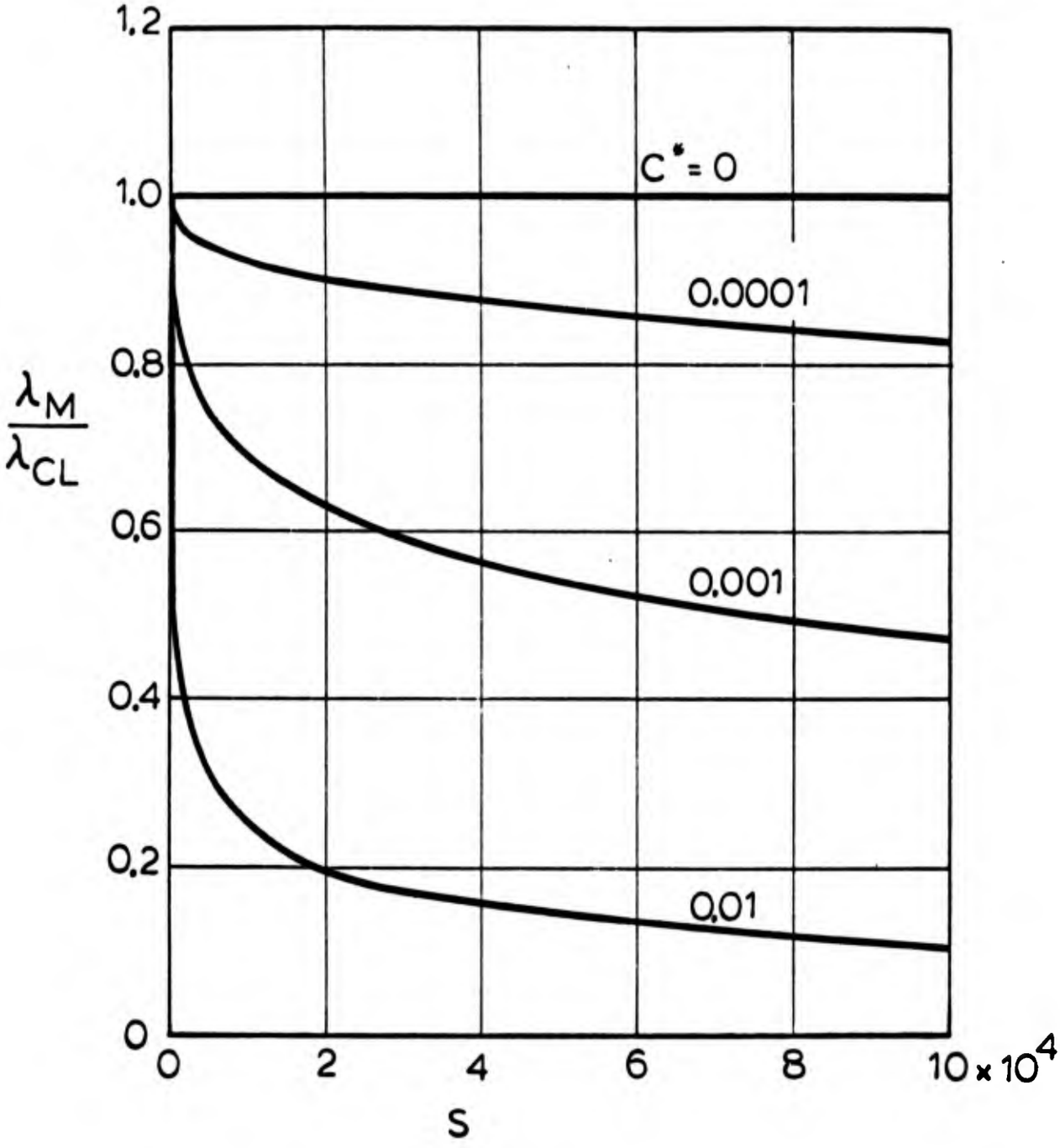

Fig. 9 Critical Load vs Imperfection Sensitivity

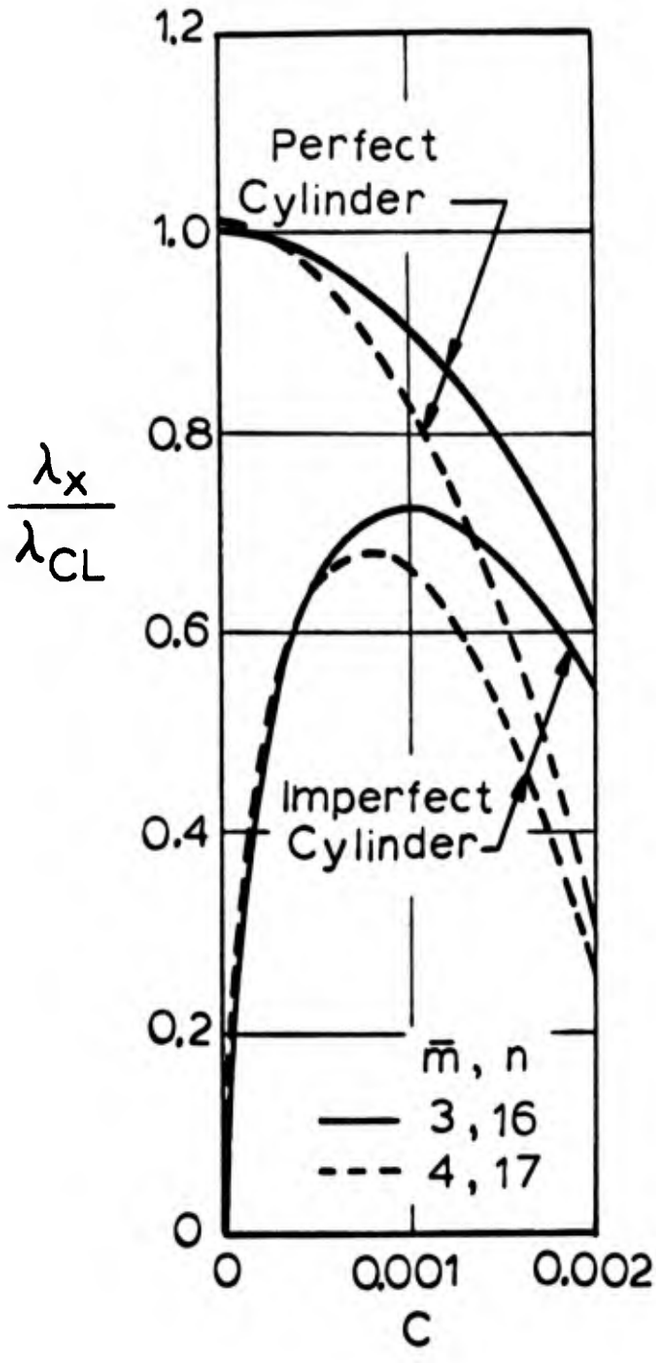

$L/R = 1$

$R/t = 400$

$\alpha_1 = 0$

$\alpha_2 = 0$

$\alpha_3 = 1.036$

$\alpha_4 = 1$

$\alpha_5 = 0.633 \times 10^{-6}$

$\alpha_6 = 0.521 \times 10^{-6}$

$\alpha_7 = 1.042 \times 10^{-6}$

Fig. 10 Influence of Mode Shape

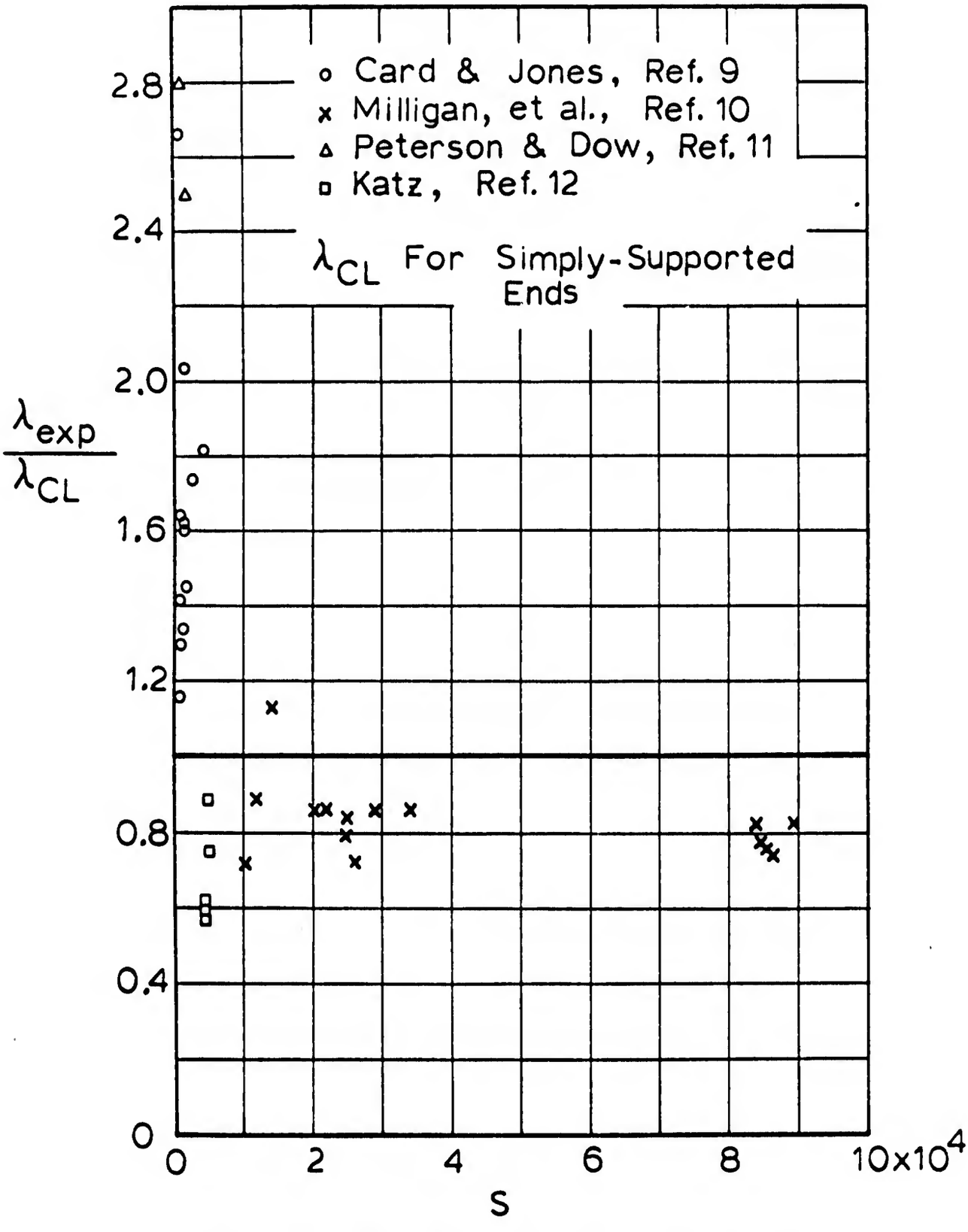

Fig. 11(a) Test Data for Stringer Stiffened Cylinders

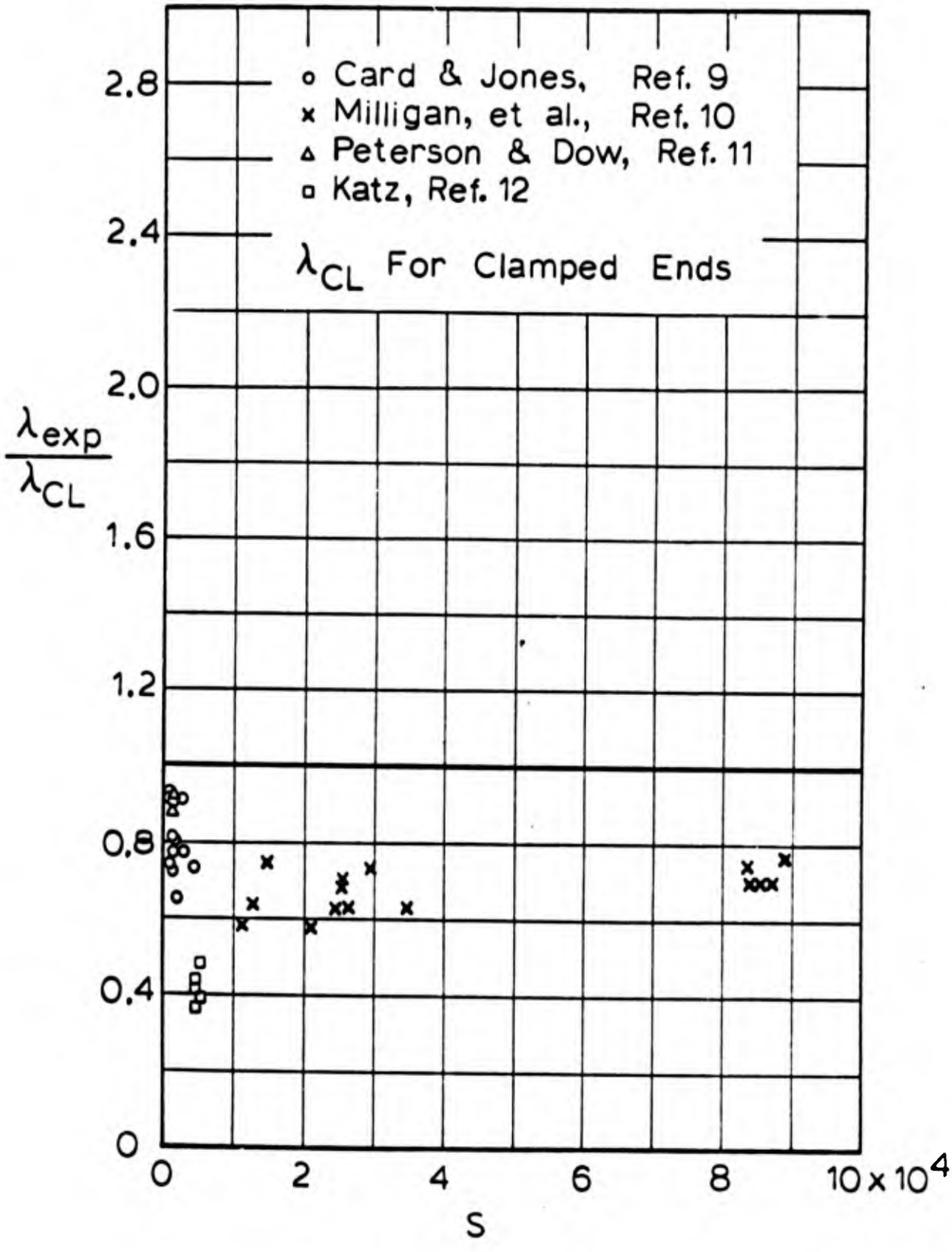

Fig. 11(b) Test Data for Stringer Stiffened Cylinders